Towards a space-borne quantum gravity gradiometer: progress in laboratory demonstration

Nan Yu, James M. Kohel, James R. Kellogg, and Lute Maleki
Jet Propulsion Laboratory
California Institute of Technology
4800 Oak Grove Drive, Pasadena, CA 91109

***Abstract*— Recent progress in atom interferometry has lead to a new way to map and monitor the Earth gravity field. Atom interferometer-based instruments may significantly contribute to the understanding of the solid earth, ice and oceans, and dynamic processes in a comprehensive model of our planet. We are funded under the Advanced Technology Component program to develop this technology for a possible flight-based gravity gravimeter. The first step of the development is a demonstration of a laboratory-based gradiometer employing component technologies suitable for a future flight instrument. This paper describes the working principles and technical benefits of atom-wave interferometer-based inertial sensors, and gives a progress report on the development of a quantum gravity gradiometer for space applications at JPL.**

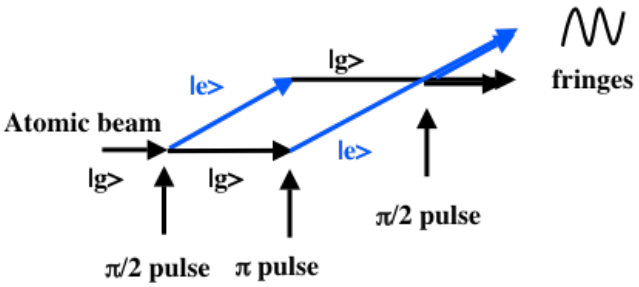

Fig. 1. Illustration of a Mach-Zehnder atom interferometer with light pulsed as atom wave optics.

I. Introduction

The recent advent of laser cooling and manipulation of atoms has lead to an entirely new class of gravity sensors: quantum gravity gradiometer (QGG) based on atom interferometer. Unlike any previously known gravity measurement techniques such as used in GRACE and GOCE missions [1], [2], the quantum gravity gradiometer uses atoms themselves as drag-free test masses. At the same time, the quantum wave-like nature of atoms is utilized to carry out interferometric measurement of the effect of gravity on the atoms. The exquisite sensitivity potentially achievable with atom-wave interferometry holds great promise for new gravity mapping and monitoring capabilities — higher measurement sensitivity, finer spatial resolution, and temporal monitoring. All these will provide new gravity measurement opportunities for the Earth Observing System in understanding the planetary inner structure and dynamics, changes in ice sheets and ocean currents, changes in underground water storage, and in overall scientific geodesy study.

In this paper, we will review briefly the principles of the quantum gravity gradiometer and its advantages in space environment. We will then describe our laboratory experiment and present an update on the gravity differential measurement and other system performance characterizations.

II. Atom Interferometer Gravity Gradiometer

The fundamental concept of atom interferometry and its use as inertial sensors have been described in the literature [3]–[6]. Briefly, one exploits the wave-like nature of atoms to construct an atom interferometer analogous to laser interferometers. One of the approaches to split and recombine atom wave is using light pulses [3], as shown in Fig. 1. It works on the basis that photons carry momentum. When an atom absorbs/emits a photon, its momentum changes accordingly. Therefore, one starts with a $\frac{\pi}{2}$ laser pulse that puts the atom in an equal superposition of the ground and excited states. While the excited state of the atom changes its momentum due to the photon absorption, the ground state remains unchanged, thus accomplishing the atom-wave beam splitting. Similarly, a π-pulse exchanges the states, functioning as a mirror in redirecting the atom wave. Therefore, a sequence of $\frac{\pi}{2}$–π–$\frac{\pi}{2}$ pulses realizes a Mach-Zehnder type interferometer as shown in Fig. 1.

In the absence of the gravity, the two paths of the interferometer arms are identical and no relative phase shifts result. If, on the other hand, atoms experience an acceleration g during this time, a net phase difference is accumulated. This phase difference can be shown to be $\Delta\phi = kgT^2$, where the interrogation time T is the time between the light pulses, and k is the effective laser wavenumber [3]. It is clear in the figure above that the atom internal states have one-to-one correspondence to the paths of the atom beam. Therefore, the fringe of the interferometer can be read out by monitoring the relative populations of the two states via laser-induced fluorescence. Knowing the laser wavenumber and the interrogation time, the gravity acceleration g can be absolutely determined.

To illustrate the sensitivity in this measurement, let's consider Cs atoms with a transition wavelength of 852 nm: with 1 s interrogation time, a mere $7 \times 10^{-9} g$ of the gravity acceleration will cause a fringe phase shift of one full radian in a single measurement. The overall measurement sensitivity

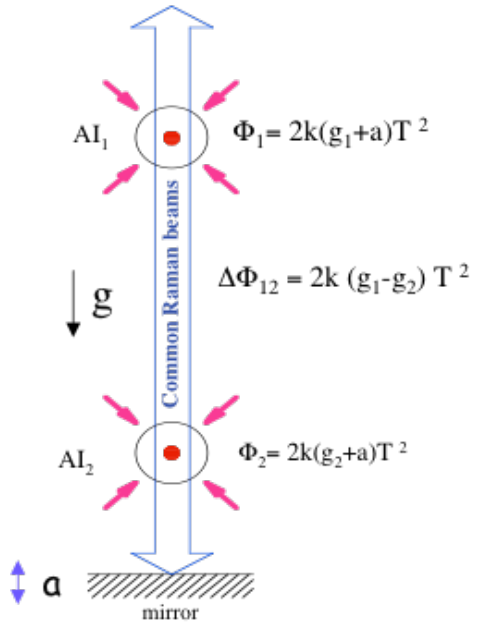

Fig. 2. Illustration of two magneto-optical traps and the configuration as a gravity gradiometer. The small shaded arrows designate the counter-propagating MOT beams with the dots as trapped atom clouds. They share the same Raman laser beams for high common-mode noise rejection

will depend on the readout signal-to-noise ratio (SNR), which is primarily determined by the atom number shot noise. A shot-noise-limited SNR greater than 1000 per atom launch has been demonstrated [7]. This would imply a sensitivity better than $10^{-11}g$ for $T = 1$ s.

Although the gravitational acceleration can be measured directly as described above, this measurement requires an inertial frame of reference which is very difficult to realize even in a controlled laboratory environment. This difficulty is rooted in Einstein's Equivalence Principle, which states that one cannot distinguish the reference frame acceleration from the gravitational acceleration in a local measurement. Gravity gradiometry then provides a more fundamental scheme of the gravitational field. A gradiometer measures the gravitational acceleration difference between two locations with a common reference frame. Other inertial accelerations are rejected as common-mode noise. The simplest implementation of a QGG consists of two atom-interferometer accelerometers separated by some distance, as illustrated in Fig. 2. The two acceleration measurements are performed simultaneously and by using the same atom interferometer laser beams, so that the common-mode noise and uncertainties are effectively cancelled [8]. With this configuration in a laboratory setting, a gravity gradient sensitivity of 10 E/Hz$^{1/2}$ (gravity gradient unit 1 E $= 10^{-9}$ s^{-2}) has been demonstrated with an effective common-mode rejection of 140 dB [8].

Impressive as the laboratory demonstrations were, the most significant gains in sensitivity result from the operation of the atom interferometer gravity gradiometer in space. As discussed before, the gradiometer sensitivity increases with the square of the interrogation time, in contrast to the $1/T$ increase in precision with most other precision measurements such as atomic clocks. In a ground-based experiment in an atomic fountain, the interrogation time is limited to a fraction of a second due to practical limitations in the physical height of the apparatus. When operating a similar experiment in a microgravity environment, the atoms will be truly drag-free. This allows much longer interrogation times in a compact apparatus, and accordingly an inertial sensitivity much higher than is possible on the ground.

When the interrogation time becomes too long, one starts to lose the number of atoms due to the finite temperature of the cold atom cloud. The atom cloud volume expands as T^3. In the worse case of the atom loss limit, the SNR goes down as $T^{-3/2}$. As a result, the phase shift for a given acceleration goes as $T^{1/2}$. In other words, one continues to gain the sensitivity by going to longer interrogation time even as one loses a greater number of atoms. Laser cooling can reduce the atom temperature to about 2 μK, which corresponds to a mean atom velocity of 2 cm/s. For example, a 10 s interrogation time in space with a modest SNR of 100 will have $10^{-13}g$ in a single measurement sequence of the accelerometer. A gradiometer with a baseline separation of 10 m would give a corresponding sensitivity about 3×10^{-4} E per single measurement, or roughly 0.001 E/Hz$^{1/2}$. New cooling and atom interferometer techniques demonstrated more recently [9], [10] will further improve overall performance.

The potential sensitivity achievable allows the gravity measurement done on board a single spacecraft. In addition, there are other salient features about the atom interferometer technology. As mentioned earlier, all atomic test masses are identical and truly drag-free in ultra-high vacuum. The phase shift due to acceleration is determined by the Raman laser wavelength, allowing on-board self-calibration. Therefore, high system stability and accuracy is expected. Atom are cooled by means of laser. The entire system operates at room temperature without the need of cryogenics. Furthermore, all operation and control are accomplished optically or photonically. The entire system is practically free from mechanical moving parts.

III. Experimental Setup

The present laboratory gradiometer consists of two atom interferometer accelerometers separated by 1 m in the vertical direction. Each accelerometer operates in an atomic fountain configuration. The fountain is needed for the laboratory system in the presence of the large gravity acceleration. The fountain configuration allows twice the interaction time for a given launch height. The atomic fountains are housed in ultra-high vacuum (UHV) enclosures, which make the core part of the atomic physics packages (APP). Our two APPs are configured differently due to the lab heritage and budget limitations. The first one, referred as APP1, is based on a vacuum system constructed from commercial off-the-shelf parts as a first testbed. It operates as a Cs vapor cell, and atoms are collected and trapped from the Cs background vapor. The Cs background pressure is about few parts 10^{-9} Torr. The vacuum enclosure has separate state-preparation and detection regions with optical access windows. One of the main drawbacks of

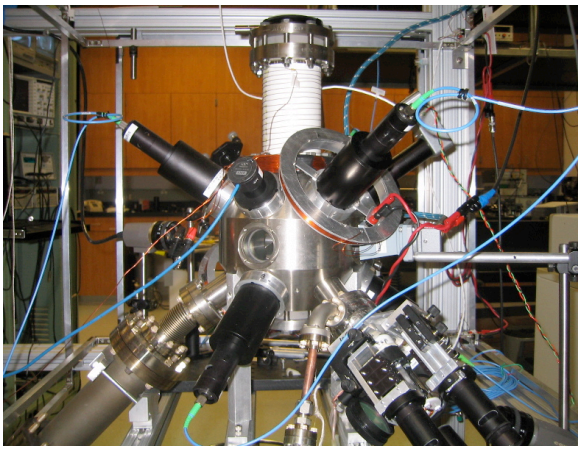

Fig. 3. Photograph of the all-Ti vacuum chamber with the attached compact source in APP1.

the vapor cell fountain is the presence of the background Cs in the detection region, which results in a detection background that degrades the SNR. We have previously reported our demonstration of an atom interferometer based on this system [6].

We recently designed and acquired an all-titanium (Ti) vacuum enclosure with welded optical windows. This enclosure was designed to offer the flexibility and allows a comprehensive system requirement study. The Ti chamber is shown in Fig. 3. It has a set of high-quality windows along the [1,1,1] axes for the magneto-optic trap (MOT) beams. There are additional three windows and three vacuum pump ports inter-spaced between these six windows. Four more windows are located in the mid-plane 90 degrees apart. Many of these additional windows are for diagnostic purposes; only eight of the thirteen windows are necessary for typical operation. Two separate large 3-in diameter windows are located on the top and bottom for the Raman laser beams for interferometry. These are high-quality $\lambda/20$ windows vacuum-sealed with copper knife-edge gaskets [11]. This sealing technique has proved to be robust in the laboratory apparatus. In this APP, we use a newly developed compact cold atom source in a separate and differentially-pumped region for loading atoms into the UHV MOT [12], where the background Cs pressure were maintained below 10^{-10} Torr.

In addition to the use of a separate compact source of cold atom beam, we also developed a new scheme of operating the atomic fountain. In this scheme, the processes of the atom state-preparation and the final state detection are all performed in the same MOT region using the same MOT laser beams. This mode of operation not only greatly simplifies the atomic fountain vacuum enclosure configuration and laser beam requirements, but also more closely corresponds to the microgravity configuration where it's not necessary to "launch" atoms to obtain long interrogation times.

Aside from the two atomic physics packages, the other major part of the gradiometer setup is the laser and optics subsystem (LOS). The LOS generates all the necessary laser

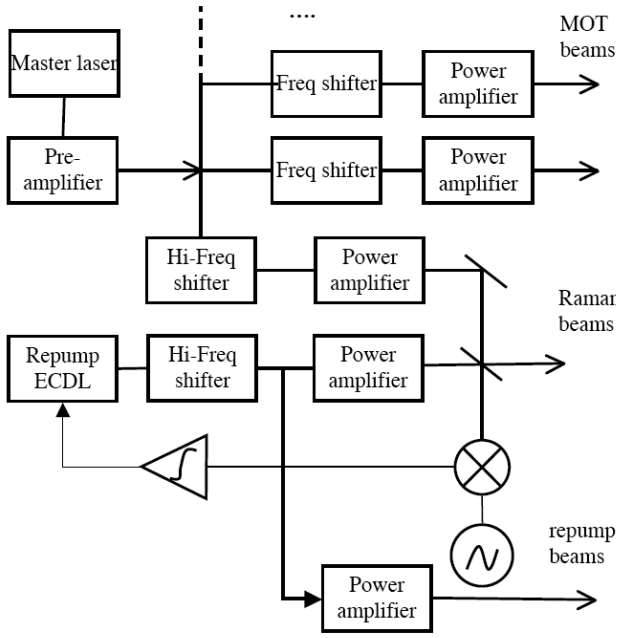

Fig. 4. Laser and optics configuration diagram.

beams required to operate the two atomic fountains plus the interferometer Raman laser beam pairs, a total of more than 20 laser beams with independent frequencies and intensities. The basic laser system configuration block diagram is shown in Fig. 4. All laser frequencies are referenced to a single master laser at the Cs $F = 4 \rightarrow 5'$ laser cooling transition. The master laser consists of a low power external cavity diode laser (ECDL) frequency-locked to the Cs atomic transition with good short and long-term stability [12]. The master laser is then pre-amplified by injection-locking a higher-power (50 mW) slave laser. From this pre-amplified laser beam, various laser frequency shifts are made through use of acousto-optic modulators (AOMs). The frequency-shifted laser beams are subsequently power-amplified by injection locking of additional high-power (150 mW) slave lasers. There are five of these slave lasers for the two MOTs and one compact source. The $F = 3 \rightarrow 4'$ repump laser frequency is provided by a second ECDL phase-locked to the $4 \rightarrow 5'$ master laser with a frequency offset of 9.2 GHz (the spacing between the two Cs ground hyperfine states). This phase locking not only frequency-stabilizes the repump laser but, more importantly, the slave lasers from which the phase-coherent Raman laser beams are derived. The repump laser is also further power-amplified by a slave laser. The two Raman lasers are detuned from the microwave resonance by 1.05 GHz using two 1 GHz AOMs, and amplified using two additional slave lasers. The entire laser and optics system is modularized with fiber-optic

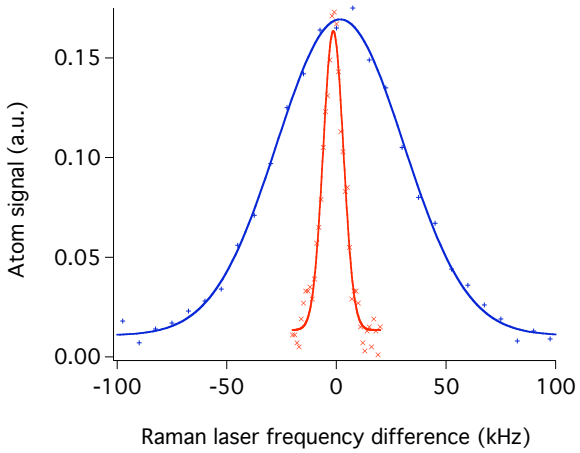

Fig. 5. Doppler sensitive Raman spectroscopy of the atom clouds before (blue line +) and after velocity selection (red line ×).

interconnections, and is contained on two $2' \times 3'$ optical breadboards [12].

A. Atom loading

Atoms are first collected and laser cooled in magneto-optical traps. In APP1, the atoms are collected directly from the background Cs vapor. The MOT consists of three pairs of 32-mm diameter laser beams. Each beam has about 8 mW of laser power. The atom loading rate is about 5×10^8 atom/s. The static number of atoms in the MOT is about 2×10^9 atoms. In APP2, however, the MOT region Cs vapor pressure is maintained below 10^{-10} Torr. A cold atom beam is generated from the 2D MOT in a separate region with relatively high Cs vapor pressure. The compact source has shown to be capable of a maximum flux of 1×10^9 atom/s. The UHV 3D MOT consists of three pairs of 24-mm diameter laser beams with about 8 mW in each beam. Currently, we are operating at a loading rate of 5×10^7 atom/s into the UHV MOT. The steady-state atom number in this MOT is about 5×10^8 atoms.

B. Launch and state preparation

After a cloud of atoms is loaded, typically in about 0.75 s, atoms are launched upwards as in an atomic fountain. The launch process starts with shutting off the MOT coils. Atoms remain in the so-called "optical molasses," and are then launched by transferring the atoms into a moving-frame molasses for about 2 ms. Before the lasers are completely turned off, further laser cooling is achieved by detuning the laser by -60 MHz while ramping down the laser intensities. We were able to achieve atom temperatures of around 2.5 μK, corresponding to a thermal velocity of less than 2 cm/s. With careful zeroing the magnetic field, atom temperatures of around 1 μK should be achievable. Fig. 5 shows the velocity profiles of the launched atoms in APP1.

Currently, our two physics packages are configured asymmetrically. In MOT1, the state preparation and detection region is 20 cm above the MOT loading region. Atoms are state-prepared in the upper region on the way up and detected on the way down. In MOT 2, on the other hand, all the actions are in a single region. Therefore, to synchronize the state preparation and detection, atoms in two MOTs are launched asynchronously. The MOT1 atoms are launched first at a higher velocity such that when the atoms reach the state preparation region their velocity matches the desired launch velocity in MOT2, and the atoms in MOT2 are launched at this instant. From this point on, the two atomic fountain trajectories are identical, and all subsequent state-preparation, Raman interferometer pulses, and detection can be performed synchronously. In typical operation, the atoms in MOT2 are launched at 1.6 m/s to give a free flight time of about 350 ms. The physical height of the chamber allows for a maximum of 600 ms of free flight time.

In order to obtain high-contrast interferometer fringes, a rather involved state preparation processes are often used [8]. Typically, one first selects the magnetic field insensitive $m_F = 0 \rightarrow 0'$ transition, then a Raman velocity selection pulse is applied. We choose to use a single Raman laser pulse to accomplish both state and velocity selection: A Raman π pulse drives the $F = 4 \rightarrow 3', m_F = 0 \rightarrow 0'$ transition while a large bias magnetic field provides a quantization axis and separates the Zeeman degeneracies. Only those atoms in the $m_F = 0$ state and within a narrow band of velocities (as determined by the Raman Rabi frequency) make the transition, and the remaining atoms are cleared by a $4 \rightarrow 5'$ resonant push beam. The total efficiency of this single-pulse process is about 0.5%. Fig. 5 shows the velocity profiles before and after velocity selection. The Raman Rabi frequency used is typically on the order of 20 kHz, while the cold atom cloud's original Doppler velocity profile is on the order of 80 kHz width. The 10 kHz width of the Doppler profile after the velocity selection implies a 1-D atom temperature of 70 nK.

This single-pulse approach simplifies the state preparation procedure and avoids the need for a separate $F = 3 \rightarrow 2'$ resonant clearing laser. The main disadvantage comes from the single-photon transitions that accompany the Raman transition. These unwanted transitions increase the background of atoms not participating in the interferometric transition and thus degrade the signal quality. Although we currently use this single-pulse state and velocity selection scheme, more efficient multi-step sequences may be employed in the future. We note that in a space-based system, the number of state-preparation steps is not limited by the transit time of the atoms as in an earth-based fountain, allowing the use of even more elaborate state preparation sequences to "recycle" atoms and maximize the efficiency of the state and velocity selections.

C. Raman pulses

The atom interferometer is realized by a pair of counter-propagating laser beams which drive the Doppler-sensitive Raman transitions [4]. In the Raman excitation process, the relative phase of the two Raman lasers is transferred to the atom wave. Any phase fluctuations result in atom interferometer fringe noise. There are a number of ways to generate the

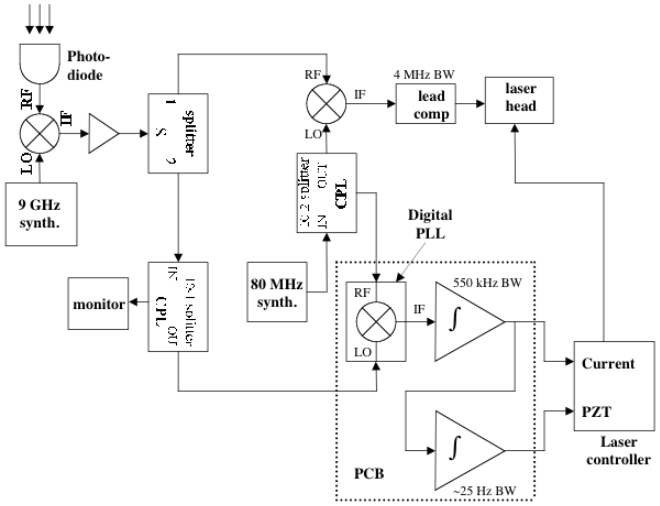

Fig. 6. The block diagram of the laser phase locking setup.

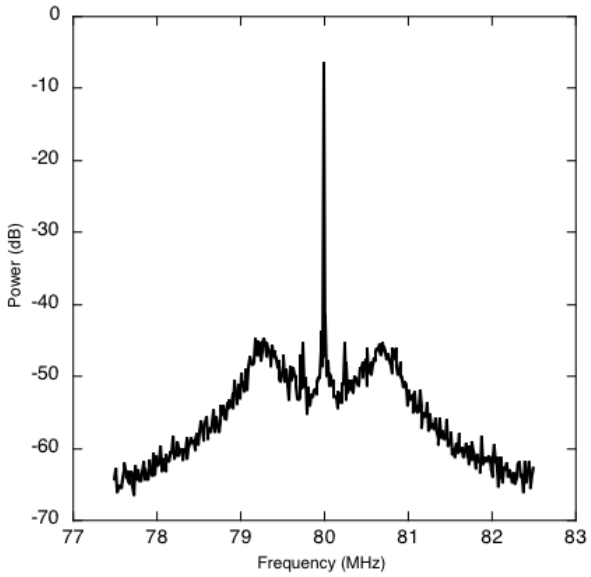

Fig. 7. The spectrum of the beatnote of the two phase locked lasers. The spectrum resolution is 1 kHz, limited by the spectrum analyzer, and the central peak contains 99% of the rf power.

phase-coherent laser pairs. We directly phase-lock one laser to another using a phase lock loop (PLL); this approach is simple, versatile and most suitable for a space-borne system.

Fig. 6 is a diagram of our phase lock loop implementation. The relative phase of the two lasers is detected by mixing the two laser fields in a fast photodetector. This beatnote is mixed down to the baseband frequency, properly filtered, and fed back to one of the laser's frequency-control input. The laser beatnote is at 9.2 GHz, the frequency offset required by the Cs hyperfine splitting. This beatnote is first mixed down to an intermediate frequency of 80 MHz. At this intermediate frequency, one can use a digital PLL device which not only provides the necessary phase discrimination but also frequency discrimination at large frequency difference, allowing a large frequency acquisition and locking range. An analog phase detector is also used in parallel for increased loop bandwidth. While this phase error is directly fed into the high-frequency current modulation port of the laser, the digital PLL signal is further integrated and goes to the lower-frequency modulation ports. The further integration of the low frequency signal increases near DC gain of the loop and ensures the true phase locking against step error signals. Fig. 7 shows the beatnote phase noise spectrum of the two lasers [12]. The relevant frequency range for the atom interferometer at the current interaction time scale is from 10 Hz to 100 kHz. Its stability is currently limited by the 80 MHz synthesizer used.

In the atomic fountain, the freely falling atoms have a constant Doppler frequency chirp of about 23 MHz/s. In the current scheme, the Doppler chirp is tracked by shifting the frequency of the 80 MHz synthesizer in the phase locking setup. We have found that our phase locking loop has a frequency slew rate on the order of 1 GHz/s, sufficient for tracking the Doppler frequency chirp.

The two Raman laser beams are combined using a polarizing beam splitter/combiner follwed by another polarizer to re-polarize the perpendicular polarizations along a single axis. The beams are delivered to the physics package through a PM fiber with the polarization oriented along one of the PM fiber axes. The fiber also service as a spatial mode filter. At the output, the Raman beams are expanded to 24 mm $1/e^2$ diameter collimated beams. The Raman laser beams are directed down from the above through the two APPs, and then retro-reflected though a quarter waveplate to produce a Lin$\perp$Lin polarization configuration. The two Raman lasers have a combined intensity of about 5 mW/cm^2. The maximum Raman transition Rabi frequency was found to be 50 kHz. The relative laser intensities were adjusted to minimize the Raman laser-induced Stark shifts. The same Raman lasers used for interferometry can also be configured to induce Doppler-free transitions. These Doppler-free transitions are useful for characterizing the intrinsic SNR and systematics such as second-order Zeeman shifts and Stark shifts. Fig. 8 shows a Doppler-insensitive clock transition of Ramsey fringes. It was generated with two Raman $\pi/2$ pulses of 75 μs separated by 1 ms. The fringe quality is similar when the number of atoms is reduced by 100.

D. Signal detection

The phase shifts in the atom interferometer signal are detected as a modulation of the relative populations in the two hyperfine ground states. The Raman interferometer pulses transfer atoms from the $F = 3$ ground state, where they were left by the state-preparation sequence, to the $F = 4$ state. We then measure the $F = 4$ ground state population via the laser-induced fluorescence from a standing-wave (SW) probe laser resonant with the $4 \rightarrow 5'$ cycling transition. To reduce the noise due to shot-to-shot variations in atom number, the signal is normalized to the total atoms in both $F = 3$ and $F = 4$ states. The laser scattering background is also

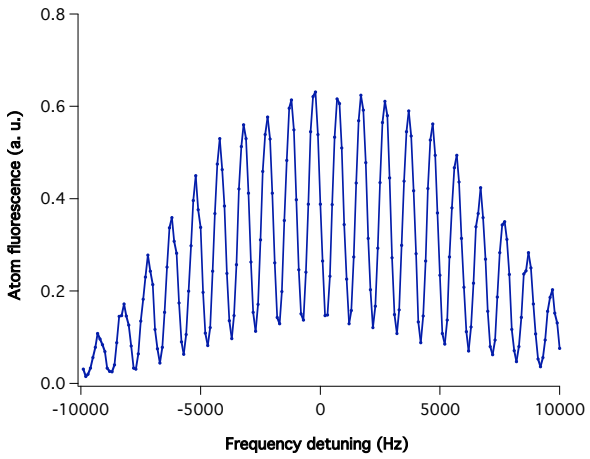

Fig. 8. Ramsey fringes resulting from Doppler-insensitive transitions.

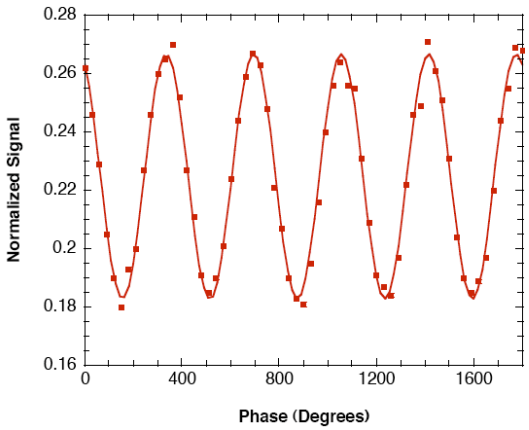

Fig. 9. Atom interferometer fringes from APP2. The total interaction time for the interferometer pulse sequence was 1 ms. Dots are unaveraged experimental data and the line a sinusoidal fit.

subtracted. Therefore, the detection sequence consists of five laser pulses: The first $4 \rightarrow 5'$ SW detection pulse measures the population in the upper ground state. A $F = 3 \rightarrow 4'$ repump pulse then transfers all atoms into the $F = 4$ state, and second $4 \rightarrow 5'$ SW detection pulse determines the total number of atoms. A $4 \rightarrow 5'$ traveling-wave push pulse follows to clear away all the atoms, and a third $4 \rightarrow 5'$ SW pulse finally measures the background due to light scattering in the absence of the cold atoms. The SW and TW pulses in the SPP2 are all generated from combinations of the upper and lower MOT beams. The background scattering in APP1 is much higher due to resonant scattering from the higher vapor pressure of thermal Cs atoms. This resonant background is negligible in APP2, which is one of the main advantages in using a UHV MOT loaded from a slow atom beam. Currently, the detection resolution is at 100 atoms, which is only limited by the slow DAC board used. We have demonstrated a SNR of 13 with 1400 total detected atoms. This will allow us to reach the atom shot noise with 10^4 detected atoms.

E. Differential acceleration measurement

Fig. 9 is a demonstration of the signals obtained from a single atom interferometer. The interferometer fringes were observed by varying the relative phase of the final $\pi/2$ pulse. At present time, we have not implemented vibration isolation for the retro-reflecting mirror. As a result, the fringe contrast degrades quickly as the interaction time increases due to environmental noise. This is precisely why the differential measurement is useful in characterizing the gravity field.

We were also able to demonstrate the simultaneous operation of the two atom interferometers. Unfortunately, the differential measurement is currently limited by the signal-to-noise in the testbed system APP1. We are working to improve the SNR in APP1, and to implement vibrational isolation for the retro-reflector platform. We expect to be able to operate the atom interferometers with interaction time of 100 ms or more in the near future, with a predicted SNR of 200. This will give an acceleration measurement sensitivity in the range of $10^{-9}g$ per measurement. Assuming two identical accelerometers separated by 10 m, the extrapolated gravity gradient sensitivity would be at 1×10^{-9} s^{-2}, or 1 E per measurement level.

F. Systematic effects

The atom interferometer-based instrument under study has the potential to offer the most stable and precise gravity gradient measurement. Nevertheless, there exists a number of intrinsic systematics which will determine the ultimate system performance. Two well-known effects are the Zeeman and Stark shifts associated with the atomic levels involved. The Zeeman effect is well studied in the atomic clock community. In fact, the controlled second-order Zeeman shift can be used to bias one of the atom interferometers such that the two atom interferometer fringes are exactly in phase. This is a requirement needed to achieve high common mode rejection [8]. The Stark shift has also been studied in the atom interferometer context, particularly in the precise photon recoil measurements [13]. There also exists some common mode rejection of the Stark shift in the differential measurement. The differential measurement also eliminates other common-mode noises such as the relative Raman laser phase jitters, similar to the rejection of vibration of the platform.

We consider here another source of systematic error. The gravity gradient is obtained by differential measurement of acceleration Δa separated by a baseline distance d, $\Delta a/d$. The precision of the gravity gradient measurement depends not only on the sensitivity of the individual accelerometers, but also the precise knowledge of the separation of the two accelerometers. Given the fact that the static gravity gradient ranges from 1500 to 3000 E, a precision of 10^{-3} E would mean that the distance is controlled to about one part per million. This is challenging issue for short baseline

gradiometers. This may prove specially challenging for the atom interferometer scheme where a cloud of atoms is used.

As the expanding cold atom cloud is characterized by certain spatial extent, an average value of acceleration is measured. This average value depends not only on the centroid position of the cloud, but also its drift velocity and cloud shape. We can easily show that the error in measured average value of the gradient Γ_0 in a constant gradient field is given by

$$\frac{\delta\Gamma}{\Gamma_0} = \frac{\langle\delta d\rangle}{d_0} + \frac{2}{3}\frac{\langle\delta v\rangle T}{d_0} \quad (1)$$

where $\langle\delta d\rangle$ and $\langle\delta v\rangle$ are the relative fluctuations of the centroid and the drift velocity of the atomic clouds, and $2T$ is the total interferometer interaction time. Clearly, any change in position, velocity distribution, and shape would result in an error in the gradient measurement. For example, to achieve 10^{-3} E precision with a 10 m baseline separation and assuming a total interaction time of 20 sec, the relative cloud centroid separation has be determined to better than 10 μm and the drift velocity difference has to be within 5 μm/s. Currently, we are studying ways to characterize and measure the stability of atomic clouds. This may indeed present a challenge to the implementation of the gradiometer to its full potential.

IV. Conclusion

An atom interferometer-based gravity gradiometer holds great promise for the Earth Sciences in geodesy, solid earth modelling, and climate and resource observation. Our goal is to develop a space-borne atom interferometer-based instrument. We have implemented a complete laboratory-based gradiometer demonstration and developed a new operational scheme feasible in space environment. We have observed high quality interferometer fringes in the system and demonstrated simultaneous fringe measurements using both physics packages. We have also identified sources of the intrinsic system instability. The expected gradiometer performance can be characterized with our current system, and we are progressing towards a gradiometer with the state-of-the-art performance by the end of the project period.

Acknowledgment

This research was carried out at the Jet Propulsion Laboratory, California Institute of Technology, under a contract with the National Aeronautics and Space Administration.

References

[1] http://www.csr.utexas.edu/grace/.
[2] http://www.esa.int/export/esaLP/goce.html
[3] M. Kasevich and S. Chu, "Measurement of the gravitational acceleration of an atom with a light-pulsed atom interferometer," Appl. Phys. B **54**, 321 (1992).
[4] M. Kasevich and S. Chu, "Atomic interferometry using stimulated Raman transitions," Phys. Rev. Lett. **67**, 181–184 (1991);
[5] Ch. J. Bordé, "Atomic interferometry with internal state labeling," Phys. Lett. A **140**, 10–12 (1989).
[6] N. Yu, J. M. Kohel, L. Romans and L. Maleki, "Quantum gravity gradiometer sensor for earth science applications," ESTC 2002, Pasadena, CA (2002).
[7] G. Santarelli *et al*., "Quantum projection noise in an atomic fountain: A high stability cesium frequency standard," Phys. Rev. Lett. **82**, 4619 (1999); J. M. McGuirk *et al*., "Low-noise detection of ultra-cold atoms," Opt. Lett. **26**, 364 (2001).
[8] J. M. McGuirk, G. T. Foster, J. B. Fixler, M. J. Snadden and Mark Kasevich, "Sensitive absolute gravity gradiometry using atom interferometry," Phys. Rev. A **65**, 033608 (2002).
[9] A. J. Kerman, V. Vuletic, C. Chin, and S. Chu, "Beyond Optical Molasses: 3D Raman Sideband Cooling of Atomic Cesium to High Phase-Space Density," Pys. Rev. Lett. **84**, p349 (2000).
[10] J. M. McGuirk, M. J. Snadden, and M. A. Kasevich, "Large Area Light-Pulse Atom Interferometry" Phys. Rev. Lett. **85**, 4498-4501 (2000).
[11] A Noble and M. Kasevich, "UHV optical window seal to conflat knife edge," Rev. Sci. Instr. **65**, pp 3042-3043 (1994).
[12] Nan Yu, James M. Kohel, Jaime Ramerez-Serrano, James R. Kellogg, Lawrence Lim and Lute Maleki, "Progress towards a space-borne quantum gravity gradiometer," ESTC 2004, June 22 to June 24, Palo Alto, CA.
[13] D. S. Weiss, B. C. Yong, S. Chu "Precions measurement of $\hbar/m_{Cs}$ based on photon recoil using laser-cooling atom interferometry," Appl. Phys. B **59**, 217 (1994).